OPTICS

Vacuum ultraviolet nonlinear metalens

Ming Lun Tseng[1,2]†, Michael Semmlinger[3,4,5]†, Ming Zhang[4,5,6]†, Catherine Arndt[3,4,5]†, Tzu-Ting Huang[2], Jian Yang[4,5,6], Hsin Yu Kuo[7], Vin-Cent Su[8], Mu Ku Chen[9], Cheng Hung Chu[2], Benjamin Cerjan[3,4], Din Ping Tsai[2,7,9]*, Peter Nordlander[3,4,6]*, Naomi J. Halas[3,4,6,10]*

Vacuum ultraviolet (VUV) light plays an essential role across science and technology, from molecular spectroscopy to nanolithography and biomedical procedures. Realizing nanoscale devices for VUV light generation and control is critical for next-generation VUV sources and systems, but the scarcity of low-loss VUV materials creates a substantial challenge. We demonstrate a metalens that both generates—by second-harmonic generation—and simultaneously focuses the generated VUV light. The metalens consists of 150-nm-thick zinc oxide (ZnO) nanoresonators that convert 394 nm (~3.15 eV) light into focused 197-nm (~6.29 eV) radiation, producing a spot 1.7 μm in diameter with a 21-fold power density enhancement as compared to the wavefront at the metalens surface. The reported metalens is ultracompact and phase-matching free, allowing substantial streamlining of VUV system design and facilitating more advanced applications. This work provides a useful platform for developing low-loss VUV components and increasing the accessibility of the VUV regime.

INTRODUCTION

Vacuum ultraviolet (VUV) light spans the wavelength range of nominally 100 to 200 nm (6 to 12 eV). VUV radiation is useful for many applications ranging from materials characterization (*1*–*6*) and processing (*7*) to biotechnology (*8*, *9*), due to its high photon energy and strong light-matter interactions. Currently, the lack of low-loss optical components and compact coherent sources is a key limiting factor in the emergence of new applications for light in this wavelength range. Virtually almost all types of glass used for conventional lenses are unsuitable for the VUV due to their strong absorption in this region (*10*). The few VUV-transmittable materials currently used for lenses, most notably CaF_2 and MgF_2, are comparably fragile, placing practical limits on thin lens fabrication and design. Reflective optics eliminate strong VUV absorption but significantly increase the bulk and complexity of VUV systems. Coherent VUV light sources have historically been large, fixed-wavelength excimer lasers requiring large laboratory footprints and substantial gas-handling equipment. Solid-state laser sources combined with nonlinear optical processes have provided expanded access to coherent VUV light. Strategies from cascaded frequency tripling in rare gas vapors (*11*, *12*) to highly cascaded harmonic generation (*13*) are methods for converting low photon energy coherent sources into this higher photon energy range. Higher-efficiency upconversion processes, such as second harmonic generation in nonlinear optical crystals, are severely constrained by the limits of phase-matching at VUV wavelengths (*14*) and also by optical absorption (*15*). New approaches to both VUV light generation and manipulation are clearly needed to advance our utilization of this region of the electromagnetic spectrum.

Metasurfaces provide a promising platform to address some of the current limitations and challenges of this wavelength range. Metasurfaces consist of subwavelength nanoresonators (meta-atoms) with well-tailored geometric parameters to achieve targeted functionalities (*16*–*21*) such as light wavefront control (*18*, *22*–*27*) and tunable light manipulation (*28*–*32*). Nonlinear metasurfaces are highly compact flat-optical components, with enhanced local effective nonlinearities that can generate VUV light without the constraint of phase matching. Because of their ability to focus incident light into nanoscale hotspots, metasurfaces can boost the efficiency of nonlinear processes and serve as compact light generation devices from the infrared to the deep-UV range (*33*–*37*). In previous work, we extended the operational wavelength of nonlinear metasurfaces into the VUV range by designing meta-atoms composed of precisely patterned nonlinear materials to support resonant modes at the desired fundamental wavelength. In the initial demonstrations of nonlinear metasurfaces for VUV generation (*38*, *39*), the generated light was dispersed into divergent patterns due to the meta-atom geometry. This diffraction is not desirable for practical applications, because additional VUV optical elements would be required for collecting and collimating the generated VUV light, inevitably introducing loss and substantially increasing the system's size. Here, we report a nonlinear metalens capable of simultaneously generating and focusing VUV light. This metalens provides a compact method for nonlinear VUV generation and focusing of the generated light eliminating the need for additional optical elements.

RESULTS

Nonlinear metalens design

A schematic of the VUV metalens is shown in Fig. 1A. It is composed of an array of meta-atoms with a Mie-type resonance (*17*) at the excitation wavelength (394 nm). As in our previous studies of VUV light generation, ZnO is used as the constituent material (*38*). The geometric parameters of the meta-atoms are provided in Fig. 1B. To manipulate the nonlinear wavefront emitted by the metalens, it is essential to have control over the harmonic wave's

[1]Institute of Electronics, National Yang Ming Chiao Tung University, Hsinchu 300, Taiwan. [2]Research Center for Applied Sciences, Academia Sinica, Taipei 115, Taiwan. [3]Department of Electrical and Computer Engineering, Rice University, Houston, TX 77005, USA. [4]Laboratory for Nanophotonics, Rice University, Houston, TX 77005, USA. [5]Applied Physics Graduate Program, Rice University, Houston, TX 77005, USA. [6]Department of Physics and Astronomy, Rice University, Houston, TX 77005, USA. [7]Department of Physics, National Taiwan University, Taipei 10617, Taiwan. [8]Department of Electrical Engineering, National United University, Miaoli 36003, Taiwan. [9]Department of Electrical Engineering, City University of Hong Kong, Kowloon, Hong Kong. [10]Department of Chemistry, Rice University, Houston, TX 77005, USA.
*Corresponding author. Email: dptsai@cityu.edu.hk (D.P.T.); nordland@rice.edu (P.N.); halas@rice.edu (N.J.H)
†These authors contributed equally to this work.

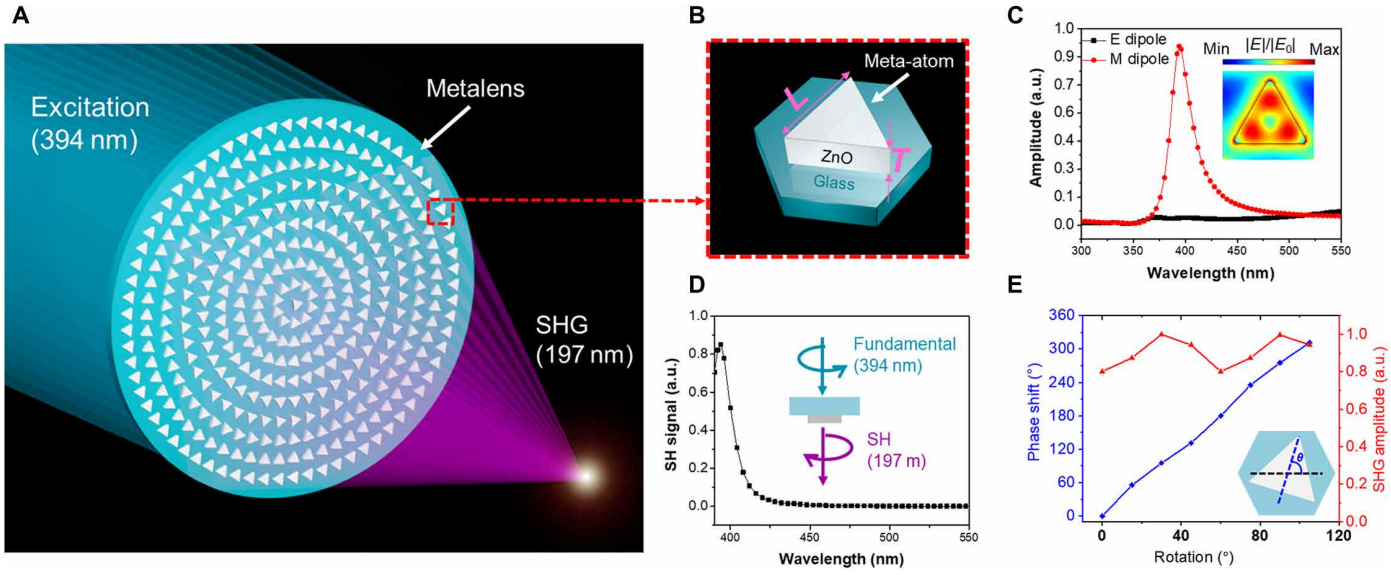

Fig. 1. VUV nonlinear metalens design. (**A**) Idealized schematic. (**B**) Geometric parameters of each meta-atom: edge length (*L*), 205 nm; thickness (*T*), 150 nm. The meta-atoms are arranged in a hexagonal lattice with a lattice constant of 270 nm. (**C**) Theoretical calculation of resonance amplitudes for electric dipole (E-dipole) and magnetic dipole (M-dipole). Inset: Simulation of the electric field enhancement within the meta-atom. (**D**) Simulation of the SHG signal versus the excitation wavelength. (**E**) Simulation of the phase modulation and nonlinear output intensity versus rotation angle at the SHG wavelength (197 nm). Blue curve and axis: Simulated nonlinear phase modulation. Red curve and axis: Simulated amplitude of SHG wave. a.u., arbitrary units.

local phase along the metalens plane. One effective approach is to introduce a nonlinear geometric phase (Pancharatnam-Berry phase) (*40*), which can effectively control the phase of the output harmonic signals under circularly polarized (CP) excitation, into the design. To efficiently generate VUV light under such an excitation conditions, each meta-atom unit cell must have a specific rotational symmetry (*34*). The rotational symmetry can be selected through consideration of the nonlinear selection rule proposed by Bloembergen (*34*, *41*) (also see the Supplementary Materials). It describes the requirements of the crystal structure's (also artificial structures') rotational symmetry for a certain harmonic order under CP light excitation. For second harmonic generation (SHG), the meta-atoms are required to have C_3 rotational symmetry (see section SI for a more detailed discussion on this topic) and are chosen to be triangularly shaped (Fig. 1B). In this work, SHG is used for VUV generation and focusing. Therefore, the meta-atoms of the nonlinear metasurfaces must have C_3 rotational symmetry under CP excitation (see section SI). To satisfy this requirement and effectively harvest the excitation into the nonlinear material, triangularly shaped meta-atoms that support strong resonances were selected as the meta-atoms (Fig. 1B).

The linear and nonlinear properties of the meta-atoms were designed and simulated via tuning their geometry using finite-element analysis (COMSOL Multiphysics). Modal decomposition (Fig. 1C) was performed (*42*), and the result shows a magnetic dipole resonance excited in the meta-atoms under 394-nm CP laser illumination. At the resonance at 397 nm, the strong light confinement in the ZnO meta-atoms is observed and allows the effective enhancement of the light-matter interaction within the meta-atom (Fig. 1C, inset). VUV light at 197 nm is produced from the illuminated meta-atoms by SHG. The intensity of the nonlinear signal as a function of excitation wavelength was simulated by performing a volume integral of meta-atoms' linear optical response to plane wave illumination at excitation and SHG wavelength using Lorentz reciprocity theorem (Fig. 1D). A detailed description of the simulation methods may be found in the Supplementary Materials and in the previously reported work (*38*). The SHG component with the opposite circular polarization relative to the excitation reaches a maximum intensity at the resonance wavelength of the meta-atom, whereas the component of the same handedness is suppressed. This result is in good agreement with the nonlinear selection rule for CP excitation and confirms that the SHG of ZnO can be boosted by introducing a resonance at the fundamental wavelength. Simulation results of the phase control versus rotation angle are shown in Fig. 1E. According to the theory of nonlinear geometric phase, under the CP excitation, the phase of the cross-polarized harmonic signal shows a dependence on the meta-atom's rotation angle (the inset of Fig. 1E). It can be described as $\varphi = (n + 1)\theta$, where φ is the phase of the harmonic wave, n is the nonlinear order, and θ is the meta-atom's rotation angle. As expected, rotating the meta-atom by θ degrees results in a 3θ phase shift in the output SHG wave ($n = 2$) with the opposite handedness. A full 2π phase control is achieved by rotating the meta-atom, and thus, the effective wavefront control of the proposed metalens is enabled. The rotation of meta-atoms introduces a mismatch between the axis of symmetry of the meta-atoms and the lattice, thus slightly changing the overall symmetry of the metalens periodically. As a result, the simulated SHG amplitudes vary nonmonotonically as a function of rotation angle (Fig. 1E). Further calculations show that this metalens design is tolerant with respect to SHG amplitude and phase variance (Supplementary Materials). Therefore, using the nonlinear geometric phase method for metalens design ensures full and effective control of the VUV wavefront output. The spatial phase profile for such a metalens can be described as

$$\varphi(r) = k_0(\sqrt{f^2 + r^2} - f)$$

Where r is the radial distance toward the center of the metalens (diameter: 45 μm), f is the designed focal length (120 μm), k_0 is the wave vector ($2\pi/\lambda$), and λ is the second harmonic wavelength (197 nm). The phase profile of the metalens was encoded on the surface by selecting the meta-atom rotation angle according to the required phase at various radial positions. The layout of the resulting metalens and a magnified subsection are shown in Fig. 2A. The actual metalens is 45 μm in diameter and consists of nominally 8400 ZnO nano triangles. Each meta-atom serves as a nonlinear dipole source and provides precise phase modulation for VUV light generation.

Sample fabrication

To fabricate the metalens, a 150-nm sputtered multicrystalline ZnO thin film was patterned using electron beam lithography and reactive ion etching (for details, see the Supplementary Materials). An optical image and scanning electron microscopic (SEM) images at different positions of the resulting nonlinear metalens are shown in Fig. 2 (B and C). Well-defined nanotriangles with regularly varying rotation angles can be observed in the SEM images, confirming design fidelity. A linear transmission spectrum of the metalens was measured to verify the resonance wavelength. As shown in the experimental linear transmission spectrum (Fig. 2D, purple curve), for left-handed CP (LCP) excitation, a resonance dip associated with the magnetic dipole resonance in the meta-atoms can be observed at nominally 395 nm, very close to the theoretical spectrum (Fig. 2D, green curve). To verify the nonlinear property of the metalens, its nonlinear spectrum (Fig. 2E) and power dependence of the nonlinear signal versus the excitation power (Supplementary Materials) was also measured using an experimental setup consisting of a UV monochromator and the UV photomultiplier (*39*). The details regarding the experimental setup can also be found in Materials and Methods and the Supplementary Materials. In the nonlinear spectral measurement (Fig. 2E), the fundamental signal wavelength was shifted slightly, from 394 to 397 nm, to allow the generated SHG light to have less absorption in air, thus propagating further and account for a slight shift in the linear resonance of the device (*43*). A sharp peak at nominally 198 nm, half of the excitation wavelength, can be observed, verifying the ability of this metalens to generate VUV light through SHG. In addition, the conversion efficiency of the metalens is found to be nominally 6×10^{-9}, which is comparable to the previously reported VUV-generating metasurface composed of disk-shaped ZnO meta-atoms (*38*).

Measurements

Characterization of the VUV focusing properties of our metalens is provided in Fig. 3. To record the three-dimensional profile of the

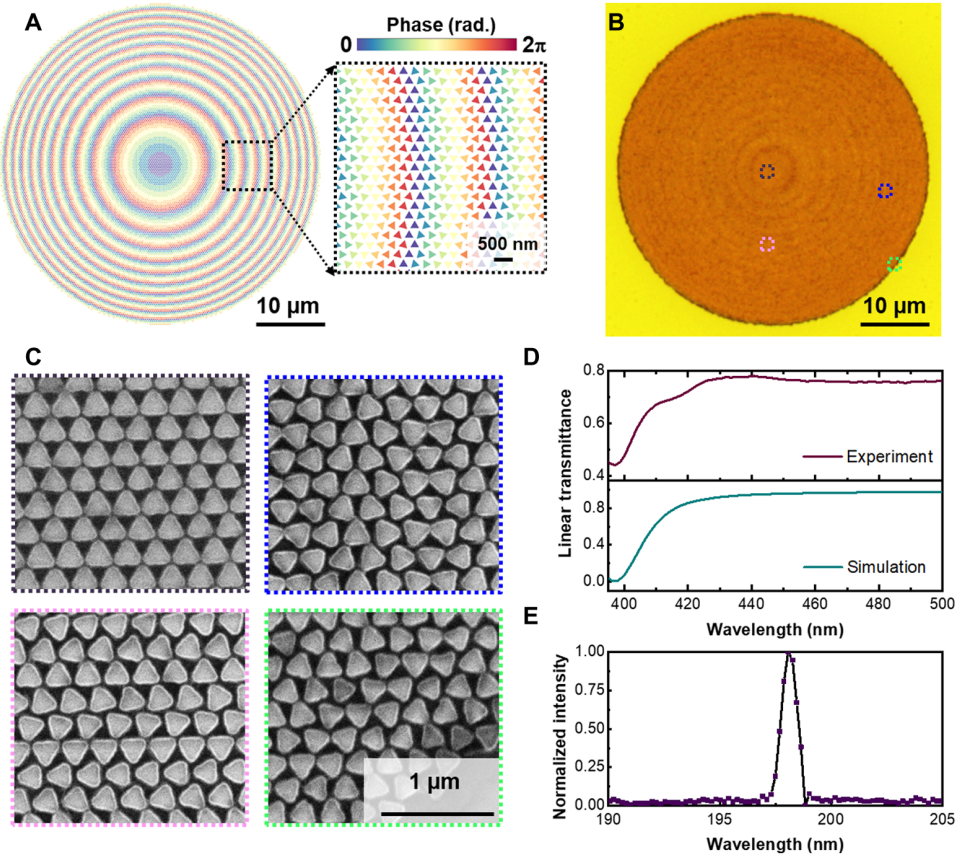

Fig. 2. Fabrication of the VUV nonlinear metalens. (**A**) Layout of the nonlinear metalens. A color code is imposed on the meta-atoms with different rotation angles to illustrate the phase profile encoded on the metasurface. An enlarged image of the phase profile is shown as the insert. (**B**) Optical microscopic image of the metalens. (**C**) SEM images of the ZnO meta-atoms at the highlighted boxes in the optical image (top right). (**D**) Linear transmission spectrum of the metalens. Top: Experimental data. Bottom: Simulation data. (**E**) Nonlinear spectral measurement. SHG spectrum of the metalens. Wavelength increment is 0.2 nm.

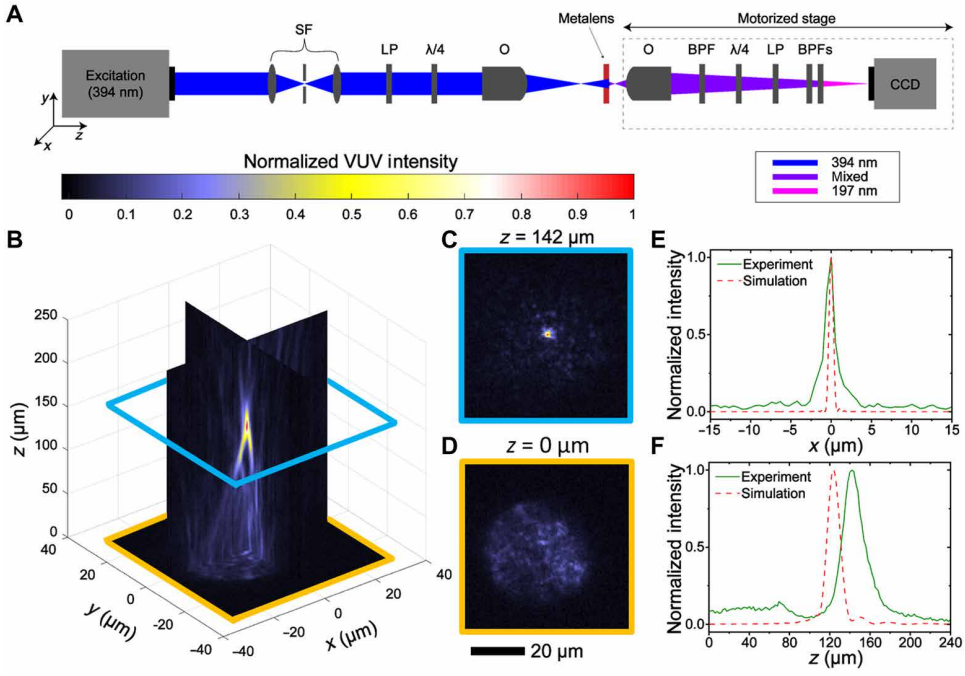

Fig. 3. Focusing measurements of the VUV nonlinear metalens. (**A**) Experimental setup. SF, spatial filter; λ/4, quarter-wave plate; LP, linear polarizer; O, objective; BPFs, bandpass filters. (**B**) Focusing profile. (**C**) Image of the focusing spot ($z = 142$ μm). (**D**) Image at metalens surface ($z = 0$). Comparison between the measured and simulated intensity cross sections of the focusing spot along the (**E**) x axis and (**F**) z axis, respectively.

VUV output, light was measured using the system depicted in Fig. 3A. A colimated LCP 394 nm laser was used as the excitation source. In the setup, an objective was used to place the focus of the excitation laser 2 mm in front of the metalens to produce a near–plane wave excitation condition. A UV objective, two bandpass filters, and a UV camera were mounted on a motorized stage to record the intensity distributions of the focused SHG along the z axis (defined in Fig. 3A). A VUV quarter-wave plate and polarizer were placed in the detection path to filter out the SHG light that was copolarized with respect to the handedness of the excitation CP light. An additional stationary bandpass filter was placed in the detection path to further reduce the fundamental signal. Additional details regarding the experimental setup can be found in the Supplementary Materials. The intensity profile of the output VUV light is shown in Fig. 3B. The figure was constructed by displaying slices of the recorded three-dimensional data in the $x = 0$ μm, $y = 0$ μm, and $z = 0$ μm planes. The zero points for the x and y dimensions were defined as the respective coordinates of the focusing point, while $z = 0$ μm was defined as the surface of the metalens image. Focusing of the SHG light can clearly be observed. An image of the VUV light at the focus ($z = 142$ μm) and at the surface of the metalens ($z = 0$ μm) are shown in Fig. 3 (C and D), respectively. As shown in Fig. 3C, at the focal plane, the focusing spot occupies only a very few pixels of the CCD.

To evaluate the metalens' capability to focus the generated VUV light, the power density at the focusing spot and the metalens plane were analyzed and compared. We estimated the maximum achievable power density for both the brightest pixel and for those pixels whose intensities fall above a threshold of 50% of the intensity of the brightest pixel. The estimated values of the average power density are 35 μW/cm^2 [peak power density per pulse (PPDPP): 0.97 kW/cm^2] for the brightest pixel, while the average values of 26 μW/cm^2 (PPDPP: 0.72 kW/cm^2) were computed for the five pixels that fell above the 50% threshold. For the metalens image (Fig. 3D), similarly, we estimated the average power density to be 1.7 μW/cm^2 (PPDPP: 0.047 kW/cm^2) using a metalens diameter of 45 μm. Therefore, it can be summarized that the power density enhancement is around 21 for the brightest pixels and around 15 for the five pixels above the 50% threshold (additional information on how the power density values were determined can be found in the Supplementary Materials) as compared to the wavefront on the plane of the metalens. According to the simulation, the metalens is capable of producing a tight, focused VUV spot with a power density more than 100 times stronger compared to the wavefront on the metalens plane, significantly larger than the 21-fold increase observed experimentally. This discrepancy is most likely due to fabrication defects of the metalens and imperfect plane wave excitation, which can be minimized in the future by further improving the fabrication and alignment processes.

Cross sections through the focus along the x and z axes and the respective simulation results are shown in Fig. 3 (E and F), respectively. The measured focus spot shows a full width at half maximum (FWHM) of 1.7 μm in the x direction and 25 μm in the z direction. To further understand the properties of the nonlinear metalens, a theoretical simulation based on scalar diffraction theory was performed (details can be found in the Supplementary Materials). The simulation shows slightly smaller FWHM values of 0.64 and 15 μm in x and z directions, respectively. The simulated focal length is 124 μm, slightly shorter than the measured value of 142 μm. The discrepancy between simulated and measured focal length may most likely be attributed to imperfections in the metalens sample itself and limitations of the experimental set up. Regarding the former, fabrication defects and the polycrystalline nature of the thin film that can lead

to additional scattering are likely key contributors. To improve the sample quality in the future, single crystalline ZnO films [e.g., those made by inductively coupled-plasma (ICP)–metalorganic chemical vapor deposition (*44*)] can be used in the fabrication. For the latter, the partially oblique incidence introduced by the Gaussian wavefront in the experiment and nonuniformities in the excitation laser beam profile contribute to the nonuniformity in Fig. 3D. Additional discussions and analysis regarding the polarization of the generated VUV light and focusing efficiency can be found in the Supplementary Materials. The versatility of our metasurface design is highlighted by its implementation in a nonlinear metasurface beam deflector that allows for control of the output direction of the SHG wave (see the Supplementary Materials). A notable advantage of this metalens over traditional VUV components is demonstrated: It effectively manipulates the SHG VUV photons in a compact space, fulfilling challenging requirements for applications such as nanolithography and VUV microscopy.

DISCUSSION

We demonstrated a VUV light–generating metalens by combining metasurface photonics with nonlinear optics through the material properties of ZnO. The nonlinear metalens consisting of ZnO meta-atoms not only serves as ultracompact nonlinear medium for VUV light generation but is also capable of effectively focusing the generated harmonic wavefront. Many interesting applications of the reported metalens can be envisioned by integration into current laser-based microscopy systems for biomedical analysis (*8*), material characterization (*4*, *6*), and nanolithography. In light of the design flexibility (*45*–*47*), additional device functionalities can be anticipated, opening the door to new and efficient VUV systems. Considering the recent demonstration of metasurface large-scale fabrication using fully complementary metal oxide semiconductor compatible processes (*48*, *49*), we believe this work illustrates a promising strategy toward high throughput manufacturing of compact VUV optical components and devices. Overall, this work lays the foundation for realizing new types of optical components for the VUV region.

MATERIALS AND METHODS

Design

The numerical simulation of linear and nonlinear properties of the ZnO meta-atom was performed by using the commercial finite-element analysis software COMSOL Multiphysics (version 5.4). In the simulation, the optical constants of ZnO are adopted from ellipsometry measurements (spectroscopic ellipsometer, HORIBA). The refractive index (n) and extinction coefficient (k) of the soda-lime glass are set as 1.5 and 0, respectively, in the linear simulation. In the nonlinear simulation, at the harmonic wavelength, the n and k of the ZnO nano-resonators (*50*) are set as 1.65 and 0.34, respectively. The exact material data for soda-lime glass at 197 nm was not found during the preparation of this paper. However, in the previous investigation (*38*), the SHG of dielectric metasurfaces are found to be insensitive to the absorptive substrate and capping layer as the energy is strongly confined in the Mie-type nanoresonators at the fundamental and harmonic wavelengths. In simulation, VUV light absorption in the soda-lime glass substrate and a refractive index shift for the substrate at 197 nm have only a moderate effect on the performance of the metalens. Therefore, the n and k of the glass substrate are set as 1.5 and 0, respectively, in the nonlinear simulation to accelerate the design process. The absorption of ZnO at 197 nm leads to a lower SHG signal strength but does not shift the resonance position (fig. S9). Periodic boundary conditions were used in the simulation. More details can be found in the Supplementary Materials.

Sample fabrication

Sputtered zinc oxide (ZnO) thin films on soda-lime glass substrates were used (provided by MTI Corporation, USA). According to the analysis based on the x-ray diffraction measurement, the average domain size in the ZnO thin film is found to be ~9.6 nm. In addition, the grain size with sizes of few tens of nanometers were found on the surface. The associated discussions on the impact of the surface roughness can be found in the Supplementary Materials. A 400-nm-thick SiO_2 layer was coated on the thin film for the subsequent electron beam lithography and dry etching processes by using plasma-enhanced chemical vapor deposition. The sample was coated with a 100-nm-thick resist ZEP-520A (Zeon Corp., Japan) on top of the SiO_2 layer, followed by coating an Espacer layer directly onto the resist-coated substrate to avoid the proximity effect due to electron scattering in the resist layer. E-beam writing was performed using an Elionix ELS-7000 electron-beam lithography system. The acceleration voltage was 100 kV, and the beam current was 100 pA. The development process was done by immersing the sample in ZEP-N50 (Zeon Corp., Japan). Subsequently, a 40-nm-thick chromium (Cr) layer was deposited using an electron-beam evaporation system, followed by the lift-off process performed in a dimethylacetamide solution (ZDMAC, Zeon Corp., Japan). Reactive ion etching was used to transfer the pattern into the SiO_2 layer. ICP reactive ion etching (RIE) (Samco Inc.) was subsequently performed. Last, the remaining SiO_2 layer was removed using the RIE System (Samco Inc.).

Measurements

The linear transmission measurement of the metalens was performed using a microspectrometer based on an inverted microscope. A halogen light source was used for the excitation. The incident light was directed to the sample using a long working distance condenser. A broadband linear polarizer and quarter waveplate were placed in the microscope to convert the polarization of the incident light into a CP state. A spectrometer box (B&W Tek Inc., BTC111E) was mounted on the microscope for spectral analysis.

For the nonlinear spectrum measurement, a frequency-doubled Ti-sapphire laser (Coherent, pulse width of 205 fs and repetition rate of 250 kHz) with an emission wavelength at 394 nm was used. A CaF_2 dispersive prism (Thorlabs, PS863) and a bandpass filter (Newport, 10LF20-193-B) were used to preseparate the SHG from the fundamental beam before entering a UV monochromator (Thermo Jarrel Ash, 2400 grooves/mm grating) equipped with a photomultiplier tube (ADIT Electron Tubes, 9781B6019).

For the metalens characterization, the setup used is shown in Fig. 3A. To improve the uniformity of excitation laser beam profile, a spatial filter consisting of a pair of lenses and a pinhole was used. The polarization of the incident laser beam was then converted into the left-hand CP (LCP) state by using a linear polarizer and a quarter-wave plate from Thorlabs. To record the focusing profile of the generated VUV light from the metalens, a UV objective (Thorlabs, LMU-15X-193) and a cooled UV camera (Princeton Instruments,

PIXIS 1024BUV) were placed on a motorized stage (Newport, ILS100CC) along the axis of the beam path. A UV quarter-wave plate (Kogakugiken Corp., Japan, VUV Achromatic QWP) and polarizer (Kogakugiken Corp., Japan, DUVGT-8) were used to filter out the part of the SHG light that was copolarized with respect to the handedness of the excitation CP light. An additional stationary bandpass filter was placed in the detection path to further reduce the fundamental signal. Additional details regarding this experimental setup can be found in the Supplementary Materials.

SUPPLEMENTARY MATERIALS

Supplementary material for this article is available at https://science.org/doi/10.1126/sciadv.abn5644

REFERENCES AND NOTES

1. L.-H. Lai, D.-C. Che, K. Liu, Photodissociative pathways of C_2H_2 at 121.6 nm revealed by a Doppler-selected time-of-flight (a 3-D mapping) technique. *J. Phys. Chem.* **100**, 6376–6380 (1996).
2. S. Leach, H.-W. Jochims, H. Baumgärtel, VUV Photodissociation of ammonia: A dispersed fluorescence excitation spectral study. *Phys. Chem. Chem. Phys.* **7**, 900–911 (2005).
3. S. Lerouge, A. C. Fozza, M. R. Wertheimer, R. Marchand, L. H. Yahia, Sterilization by low-pressure plasma: The role of vacuum-ultraviolet radiation. *Plasmas Polym.* **5**, 31–46 (2000).
4. J. A. Sobota, S. Yang, J. G. Analytis, Y. L. Chen, I. R. Fisher, P. S. Kirchmann, Z. X. Shen, Ultrafast optical excitation of a persistent surface-state population in the topological insulator Bi_2Se_3. *Phys. Rev. Lett.* **108**, 117403 (2012).
5. V. N. Vasilets, A. V. Kuznetsov, V. I. Sevastianov, Vacuum ultraviolet treatment of polyethylene to change surface properties and characteristics of protein adsorption. *J. Biomed. Mater. Res. A* **69A**, 428–435 (2004).
6. Y. Mao, D. Zhao, S. Yan, H. Zhang, J. Li, K. Han, X. Xu, C. Guo, L. Yang, C. Zhang, K. Huang, Y. Chen, A vacuum ultraviolet laser with a submicrometer spot for spatially resolved photoemission spectroscopy. *Light Sci. Appl.* **10**, 22 (2021).
7. P. Bergonzo, U. Kogelschatz, I. W. Boyd, Direct photo-deposition of silicon dioxide films using a xenon excimer lamp. *Appl. Surf. Sci.* **69**, 393–397 (1993).
8. J. Wang, Z. Wang, F. Liu, L. Cai, J. B. Pan, Z. Li, S. Zhang, H. Y. Chen, X. Zhang, Y. Mo, Vacuum ultraviolet laser desorption/ionization mass spectrometry imaging of single cells with submicron craters. *Anal. Chem.* **90**, 10009–10015 (2018).
9. T. Ito, in *Synchrotron Radiation in Structural Biology*, R. M. Sweet, A. D. Woodhead, Eds. (Springer US, 1989), pp. 221–241.
10. M. Zelikoff, K. Watanabe, E. C. Y. Inn, Absorption coefficients of gases in the vacuum ultraviolet. Part II. Nitrous oxide. *J. Chem. Phys.* **21**, 1643–1647 (1953).
11. A. H. Kung, J. F. Young, S. E. Harris, Generation of 1182-Å radiation in phase-matched mixtures of inert gases. *Appl. Phys. Lett.* **22**, 301–302 (1973).
12. R. Miles, S. Harris, Optical third-harmonic generation in alkali metal vapors. *IEEE J. Quantum Electron.* **9**, 470–484 (1973).
13. D. E. Couch, D. D. Hickstein, D. G. Winters, S. J. Backus, M. S. Kirchner, S. R. Domingue, J. J. Ramirez, C. G. Durfee, M. M. Murnane, H. C. Kapteyn, Ultrafast 1 MHz vacuum-ultraviolet source via highly cascaded harmonic generation in negative-curvature hollow-core fibers. *Optica* **7**, 832–837 (2020).
14. P. S. Halasyamani, J. M. Rondinelli, The must-have and nice-to-have experimental and computational requirements for functional frequency doubling deep-UV crystals. *Nat. Commun.* **9**, 2972 (2018).
15. L. Koller, *Ultraviolet Radiation* (John Wiley & Sons, ed. 2, 1965).
16. V. Kildishev Alexander, A. Boltasseva, M. Shalaev Vladimir, Planar photonics with metasurfaces. *Science* **339**, 1232009 (2013).
17. I. Kuznetsov Arseniy, E. Miroshnichenko Andrey, L. Brongersma Mark, S. Kivshar Yuri, B. Luk'yanchuk, Optically resonant dielectric nanostructures. *Science* **354**, eaag2472 (2016).
18. G.-Y. Lee, J. Sung, B. Lee, Metasurface optics for imaging applications. *MRS Bull.* **45**, 202–209 (2020).
19. N. Yu, F. Capasso, Flat optics with designer metasurfaces. *Nat. Mater.* **13**, 139–150 (2014).
20. M. L. Tseng, Y. Jahani, A. Leitis, H. Altug, Dielectric metasurfaces enabling advanced optical biosensors. *ACS Photonics* **8**, 47–60 (2021).
21. S. M. Kamali, E. Arbabi, A. Arbabi, A. Faraon, A review of dielectric optical metasurfaces for wavefront control. *Nanophotonics* **7**, 1041–1068 (2018).
22. M. L. Tseng, H. H. Hsiao, C. H. Chu, M. K. Chen, G. Sun, A. Q. Liu, D. P. Tsai, Metalenses: Advances and applications. *Adv. Opt. Mater.* **6**, 1800554 (2018).
23. J. Engelberg, U. Levy, The advantages of metalenses over diffractive lenses. *Nat. Commun.* **11**, 1991 (2020).
24. K. Huang, F. Qin, H. Liu, H. Ye, C. W. Qiu, M. Hong, B. Luk'yanchuk, J. Teng, Planar diffractive lenses: Fundamentals, functionalities, and applications. *Adv. Mater.* **30**, 1704556 (2018).
25. R. J. Lin, V. C. Su, S. Wang, M. K. Chen, T. L. Chung, Y. H. Chen, H. Y. Kuo, J. W. Chen, J. Chen, Y. T. Huang, J. H. Wang, C. H. Chu, P. C. Wu, T. Li, Z. Wang, S. Zhu, D. P. Tsai, Achromatic metalens array for full-colour light-field imaging. *Nat. Nanotechnol.* **14**, 227–231 (2019).
26. S. Wang, P. C. Wu, V. C. Su, Y. C. Lai, M. K. Chen, H. Y. Kuo, B. H. Chen, Y. H. Chen, T. T. Huang, J. H. Wang, R. M. Lin, C. H. Kuan, T. Li, Z. Wang, S. Zhu, D. P. Tsai, A broadband achromatic metalens in the visible. *Nat. Nanotechnol.* **13**, 227–232 (2018).
27. M. K. Chen, Y. Wu, L. Feng, Q. Fan, M. Lu, T. Xu, D. P. Tsai, Principles, functions, and applications of optical meta-lens. *Adv. Opt. Mater.* **9**, 2001414 (2021).
28. C. H. Chu, M. L. Tseng, J. Chen, P. C. Wu, Y. H. Chen, H. C. Wang, T. Y. Chen, W. T. Hsieh, H. J. Wu, G. Sun, D. P. Tsai, Active dielectric metasurface based on phase-change medium. *Laser Photonics Rev.* **10**, 986–994 (2016).
29. A. Leitis, A. Heßler, S. Wahl, M. Wuttig, T. Taubner, A. Tittl, H. Altug, All-dielectric programmable Huygens' metasurfaces. *Adv. Funct. Mater.* **30**, 1910259 (2020).
30. M. L. Tseng, J. Yang, M. Semmlinger, C. Zhang, P. Nordlander, N. J. Halas, Two-dimensional active tuning of an aluminum plasmonic array for full-spectrum response. *Nano Lett.* **17**, 6034–6039 (2017).
31. P. C. Wu, R. A. Pala, G. Kafaie Shirmanesh, W. H. Cheng, R. Sokhoyan, M. Grajower, M. Z. Alam, D. Lee, H. A. Atwater, Dynamic beam steering with all-dielectric electro-optic III–V multiple-quantum-well metasurfaces. *Nat. Commun.* **10**, 3654 (2019).
32. J. Li, S. Kamin, G. Zheng, F. Neubrech, S. Zhang, N. Liu, Addressable metasurfaces for dynamic holography and optical information encryption. *Sci. Adv.* **4**, eaar6768 (2018).
33. J. Cambiasso, G. Grinblat, Y. Li, A. Rakovich, E. Cortés, S. A. Maier, Bridging the gap between dielectric nanophotonics and the visible regime with effectively lossless gallium phosphide antennas. *Nano Lett.* **17**, 1219–1225 (2017).
34. K. Konishi, T. Higuchi, J. Li, J. Larsson, S. Ishii, M. Kuwata-Gonokami, Polarization-controlled circular second-harmonic generation from metal hole arrays with threefold rotational symmetry. *Phys. Rev. Lett.* **112**, 135502 (2014).
35. J. Lee, M. Tymchenko, C. Argyropoulos, P. Y. Chen, F. Lu, F. Demmerle, G. Boehm, M. C. Amann, A. Alù, M. A. Belkin, Giant nonlinear response from plasmonic metasurfaces coupled to intersubband transitions. *Nature* **511**, 65–69 (2014).
36. S. Liu, P. P. Vabishchevich, A. Vaskin, J. L. Reno, G. A. Keeler, M. B. Sinclair, I. Staude, I. Brener, An all-dielectric metasurface as a broadband optical frequency mixer. *Nat. Commun.* **9**, 2507 (2018).
37. P. N. Melentiev, A. E. Afanasiev, A. A. Kuzin, V. M. Gusev, O. N. Kompanets, R. O. Esenaliev, V. I. Balykin, Split hole resonator: A nanoscale UV light source. *Nano Lett.* **16**, 1138–1142 (2016).
38. M. Semmlinger, M. L. Tseng, J. Yang, M. Zhang, C. Zhang, W. Y. Tsai, D. P. Tsai, P. Nordlander, N. J. Halas, Vacuum ultraviolet light-generating metasurface. *Nano Lett.* **18**, 5738–5743 (2018).
39. M. Semmlinger, M. Zhang, M. L. Tseng, T. T. Huang, J. Yang, D. P. Tsai, P. Nordlander, N. J. Halas, Generating third harmonic vacuum ultraviolet light with a TiO_2 metasurface. *Nano Lett.* **19**, 8972–8978 (2019).
40. G. Li, S. Zhang, T. Zentgraf, Nonlinear photonic metasurfaces. *Nat. Rev. Mater.* **2**, 17010 (2017).
41. H. J. Simon, N. Bloembergen, Second-harmonic light generation in crystals with natural optical activity. *Phys. Rev.* **171**, 1104–1114 (1968).
42. T. Kaelberer, V. A. Fedotov, N. Papasimakis, D. P. Tsai, N. I. Zheludev, Toroidal dipolar response in a metamaterial. *Science* **330**, 1510–1512 (2010).
43. K. Watanabe, M. Zelikoff, E. C. Inn, "Absorption coefficients of several atmospheric gases," (Air Force Cambridge Research Labs Hanscom AFB MA, 1953).
44. J. H. Park, S. J. Jang, S. S. Kim, B. T. Lee, Growth and characterization of single crystal ZnO thin films using inductively coupled plasma metal organic chemical vapor deposition. *Appl. Phys. Lett.* **89**, 121108 (2006).
45. L. Wang, S. Kruk, K. Koshelev, I. Kravchenko, B. Luther-Davies, Y. Kivshar, Nonlinear wavefront control with all-dielectric metasurfaces. *Nano Lett.* **18**, 3978–3984 (2018).
46. T. Pertsch, Y. Kivshar, Nonlinear optics with resonant metasurfaces. *MRS Bull.* **45**, 210–220 (2020).
47. C. Schlickriede, S. S. Kruk, L. Wang, B. Sain, Y. Kivshar, T. Zentgraf, Nonlinear imaging with all-dielectric metasurfaces. *Nano Lett.* **20**, 4370–4376 (2020).
48. T. Hu, C. K. Tseng, Y. H. Fu, Z. Xu, Y. Dong, S. Wang, K. H. Lai, V. Bliznetsov, S. Zhu, Q. Lin, Y. Gu, Demonstration of color display metasurfaces via immersion lithography on a 12-inch silicon wafer. *Opt. Express* **26**, 19548–19554 (2018).
49. A. Leitis, M. L. Tseng, A. John-Herpin, Y. S. Kivshar, H. Altug, Wafer-scale functional metasurfaces for mid-infrared photonics and biosensing. *Adv. Mater.* **33**, 2102232 (2021).
50. C. H. Zhai, R. J. Zhang, X. Chen, Y. X. Zheng, S. Y. Wang, J. Liu, N. Dai, L. Y. Chen, Effects of Al doping on the properties of ZnO thin films deposited by atomic layer deposition. *Nanoscale Res. Lett.* **11**, 407 (2016).

51. K. O'Brien, H. Suchowski, J. Rho, A. Salandrino, B. Kante, X. Yin, X. Zhang, Predicting nonlinear properties of metamaterials from the linear response. *Nat. Mater.* **14**, 379–383 (2015).
52. B. H. Chen, P. C. Wu, V. C. Su, Y. C. Lai, C. H. Chu, I. C. Lee, J. W. Chen, Y. H. Chen, Y. C. Lan, C. H. Kuan, D. P. Tsai, GaN metalens for pixel-level full-color routing at visible light. *Nano Lett.* **17**, 6345–6352 (2017).
53. M. L. Tseng, Z. H. Lin, H. Y. Kuo, T. T. Huang, Y. T. Huang, T. L. Chung, C. H. Chu, J. S. Huang, D. P. Tsai, Stress-induced 3D Chiral fractal metasurface for enhanced and stabilized broadband near-field optical chirality. *Adv. Opt. Mater.* **7**, 1900617 (2019).
54. P. C. Wu, W. L. Hsu, W. T. Chen, Y. W. Huang, C. Y. Liao, A. Q. Liu, N. I. Zheludev, G. Sun, D. P. Tsai, Plasmon coupling in vertical split-ring resonator metamolecules. *Sci. Rep.* **5**, 9726 (2015).
55. P. J. Campagnola, A. C. Millard, M. Terasaki, P. E. Hoppe, C. J. Malone, W. A. Mohler, Three-dimensional high-resolution second-harmonic generation imaging of endogenous structural proteins in biological tissues. *Biophys. J.* **82**, 493–508 (2002).
56. S. Sun, K. Y. Yang, C. M. Wang, T. K. Juan, W. T. Chen, C. Y. Liao, Q. He, S. Xiao, W. T. Kung, G. Y. Guo, L. Zhou, D. P. Tsai, High-efficiency broadband anomalous reflection by gradient meta-surfaces. *Nano Lett.* **12**, 6223–6229 (2012).

Acknowledgments: We thank K. Chapkin, C. Zhang, L. Zhou, M.-H. Shih, Y.-J. Lu, R.-J. Lin, J.-W. Chen, and D. Solti for discussion and support. **Funding:** We acknowledge financial support from the Ministry of Science and Technology, Taiwan (grant nos. 107-2311-B-002 -022 -MY3, 108-2221-E-002-168-MY4, and MOST 110-2636-M-A49-001-) and National Taiwan University (NTU-107 L7728, NTU-107 L7807, and NTU-YIH-08HZT49001. We are also grateful to the Shenzhen Science and Technology Innovation Commission Grant (no. SGDX2019081623281169), the University Grants Committee/Research Grants Council of the Hong Kong Special Administrative Region, China (project no. AoE/P-502/20 and GRF project no. 15303521), the Department of Science and Technology of Guangdong Province (2020B1515120073), and the Department of Electrical Engineering, City University of Hong Kong (project no. 9380131). M.L.T. acknowledges the support from the Ministry of Education (Yushan Young Scholar Program), Taiwan. M.L.T. and D.P.T. acknowledge the Research Center for Applied Sciences, Academia Sinica, for their support in using the FIB system (FEI Helios 660 Nanolab) and the SEM/EBL system (FEI Inspect F SEM). We acknowledge support from the Robert A. Welch Foundation, C-1220 (N.J.H.) and C-1222 (P.N.), the Air Force Office of Scientific Research Multidisciplinary Research Program of the University Research Initiative (AFOSR MURI FA9550-15-1-0022) (N.J.H. and P.N.). C.A. acknowledges support from the National Science Foundation Graduate Research Fellowship Program under grant no. 1842494. **Author contributions:** M.L.T., M.S., P.N., N.J.H., and D.P.T. conceived and designed the experiments. M.L.T., J.Y., M.Z., C.H.C., and T.-T.H. designed the samples and performed the theoretical simulations. M.L.T. and V.-C.S. fabricated the samples. M.S., C.A., H.Y.K., B.C., and M.L.T. performed the inspections of the samples and the optical measurements. P.N., N.J.H., and D.P.T. supervised the research. M.L.T., M.S., C.A., Z.M., B.C., M.K.C., P.N., N.J.H., and D.P.T. prepared the manuscript. All authors analyzed the results and contributed to the preparation of the manuscript and discussions. **Competing interests:** M.L.T., M.S., M.Z., J.Y., D.P.T., P.N., and N.J.H. are inventors on a patent associated with this work (Harmonic light-generating metasurface, WO2020072502A1, EP3861404A1, and US20220011646A1). The authors declare that they have no other competing interests. **Data and materials availability:** All data needed to evaluate the conclusions in the paper are present in the paper and/or the Supplementary Materials.

Submitted 6 December 2021
Accepted 2 March 2022
Published 20 April 2022
10.1126/sciadv.abn5644